

Sn-Cu Alloy Materials with Optimized Nanoporous Structure and Enhanced Performance for Lithium-Ion Batteries Prepared by Dealloying

Chunhui Tan¹, Gongwei Qi¹, Yeping Li¹, Jing Guo¹, Xin Wang¹, Delong Kong², Hongjun Wang², Shuyong Zhang^{1,*}

¹ Key Laboratory of Colloid and Interface Chemistry, Ministry of Education, School of Chemistry and Chemical Engineering, Shandong University, Jinan, China, 250100

² Shandong Sacred Sun Power Co. Ltd. Qufu, China, 273100

*E-mail: syzhang@sdu.edu.cn

Received: 17 August 2012 / Accepted: 11 September 2012 / Published: 1 October 2012

Three kinds of binder-free nanoporous Sn-Cu alloys are prepared by electroplating followed by electrochemical dealloying and tested as possible negative electrode materials for lithium-ion battery. The morphology and structure of these alloys were characterized by X-ray diffraction, scanning electron microscopy and atomic absorption spectrophotometer. Experimental results suggest that the composition, pore size, size distribution, homogeneity of the alloys can be facilely controlled by changing the ratio of main salts in the electroplating bath. The Sn content in the alloys after electrochemical dealloying reduces significantly and Cu₆Sn₅ become the main active component. However there is no obvious decrease in specific capacity. The initial specific capacities of all the materials are in 480-810 mA h g⁻¹ range. But the capacity of as-deposited Sn-Cu alloys remain only 110-190 mA h g⁻¹ after 50 cycles, while one of the capacity of the nanoporous Sn-Cu alloys remain around 400 mA h g⁻¹ after the same cycles. This suggests that both capacity and cycling performance can be improved by optimizing the nanostructure of the materials using electrochemical dealloying.

Keywords: Lithium-ion battery, Negative materials, Sn-Cu alloy, nanoporous materials, Electrochemical dealloying.

1. INTRODUCTION

The demand of lithium-ion batteries (LIB) with higher specific capacity, better charge and discharge cycling performance and better safety continuously increases due to their wide application in portable electronic devices [1]. The negative materials of most commercial LIB are modified natural graphite. This kind of carbon materials usually gives a low maximum theoretical capacity (372 mA h

g^{-1}) and faces severe safety problems in high-rate charge and discharge processes. Therefore, a lot of efforts have been devoted to find new negative materials.

Materials with much higher theoretical specific capacity such as Sn, Si, Sb, Al, and Ge have been studied [2]. Among these materials, Sn-based materials attract attention of many researchers. However, the great volume fluctuation of pure Sn phase during charge and discharge cycling worsen its performance and shorten its duration [3, 4]. Two main approaches namely alloying and structure designing have been adopted to improve the performance of the Sn-based materials. It was found that alloying Sn with some inert metallic components such as Ni [5, 6], Cu [7, 8], Co [9, 10] can improve the cycling performance of Sn-based materials to a certain extent. Otherwise, both theoretical and experimental analysis proved that reducing particle size of Sn phase increases the active area, improves transport of electrolyte, and accelerates reaction rate [9, 11, 12]. But aggregation of nanoparticles usually deteriorates the electrode rapidly during charge-discharge cycling [12]. Some researchers turn their attention to porous materials due to their large active area, more room for volume change, higher conductivity and no aggregation.

Many approaches have been adopted to introduce pores of different scales in the active material matrix. For example, hydrogen bubbles or colloidal crystal have been used as template for preparation of porous materials [6, 10, 13, 14]. Copper foam was also used as framework for porous materials [5, 15-17]. A class of composite anode materials made of Sn or Sn alloy that were encapsulated in a conductive microporous carbon membrane or multichannel carbon microtubes were also investigated [18, 19]. Yu *et al.* developed a 3-dimension nanoporous Au supported tin foil as alternative anode for LIB and found that the capacity of this material remain 600 mA h g^{-1} after 140 cycles [20].

In this work, we attempt to combine the alloying and the porous-structuring strategies to find a facile and effective way for improving the performance of Sn-based alloy. The structure of the porous materials was controlled by changing Sn content in the electrodeposited Sn-Cu alloy. Three kinds of nanoporous Sn-Cu alloy materials were prepared by electroplating Sn-Cu alloy on one side of a piece of Cu foil substrate followed by electrochemical dealloying of part of Sn. The structural and electrochemical properties of the six alloys are compared.

2. EXPERIMENTAL

A piece of Cu foil substrate was first washed in acetone and 0.1 mol L^{-1} HCl solution before electrodeposition so as to remove the surface contamination and oxide and then dried in open air. Sn-Cu alloys were electrodeposited using pyrophosphate baths with different concentration of CuSO_4 and SnSO_4 as main salts. The compositions of the baths are listed in Table 1. Electroplating was carried out in a two-electrode cell. The Cu foil served as the cathode and a Ti foil as the anode. The area of the cathode is 10 cm^2 . Electroplating was conducted at a current density of -10 mA cm^{-2} for 10 min. Dealloying is conducted in the same cell for 10 min at a current density of 5 mA cm^{-2} with the Sn-Cu alloy on Cu foil serving as the anode and a Ni net serving as the cathode in a 1 mol L^{-1} acetic acid.

Table 1. Bath composition for electrodeposition of different Sn-Cu alloys

Bath	A	B	C
$\text{K}_4\text{P}_2\text{O}_7 \cdot 3\text{H}_2\text{O}$	192 g L ⁻¹	192 g L ⁻¹	192 g L ⁻¹
NaH_2PO_2	21.2 g L ⁻¹	21.2 g L ⁻¹	21.2 g L ⁻¹
$\text{CuSO}_4 \cdot 5\text{H}_2\text{O}$	12.5 g L ⁻¹	15.0 g L ⁻¹	17.5 g L ⁻¹
SnSO_4	32.2 g L ⁻¹	30.0 g L ⁻¹	27.9 g L ⁻¹
Gelatin	2.5 g L ⁻¹	2.5 g L ⁻¹	2.5 g L ⁻¹

Both electrodeposition and electrochemical dealloying were carried out at room temperature without stirring. After electrochemical dealloying, the products were washed with water and ethanol, and then air-dried. The as-deposited alloy samples and the nanoporous materials were marked with 1 and 2, respectively. For example, A1 and A2 corresponds to the Sn-Cu alloy directly deposited from Bath A before and after electrochemical dealloying respectively. The mass of Sn-Cu materials loaded on the Cu foil surface was obtained by weighting using an analytic balance with an accuracy of 0.1 mg.

All the reagents used in the experiments were of analytical grade, purchased from Sinopharm Chemical Reagent Co., Ltd. and used without further purification.

Test CR2025 coin cells were assembled in an argon-filled glove box at room temperature. The Sn-Cu alloy material loaded on Cu foil was used as the positive electrode and a lithium sheet was used as the negative electrode and the reference electrode. The electrolyte was 1 mol L⁻¹ LiPF₆ solution with a mixture of ethylene carbonate/dimethyl carbonate/ethyl methyl carbonate in 1:1:1 (vol. %) serving as the solvent, which was provided by Beijing Institute of Chemical Reagents. The cathode and anode were separated by a piece of Celgard 2400 membrane.

The morphology and structure of the Sn-Cu alloy materials before and after electrochemical dealloying was characterized using a JSM-7600F Field emission scanning electron microscope (SEM, JEOL, Japan) operating at an acceleration voltage of 5 kV. The composition of the alloy material was analyzed using a 3510 Atomic absorption spectrophotometer (AAS, HP, USA). The crystallographic information of the alloys was recorded using a D8 Advance X-ray diffractometer (XRD, Bruker, Germany) with Cu K α radiation at a scan rate of 0.5°s⁻¹.

The charge and discharge cycling tests were performed using a CT2001C-001 Battery testing system (Land Co., Ltd, Wuhan, China) at 0.2 C rate within a cut-off voltage of 0.05–1.5 V (vs. Li/Li⁺). Cyclic voltammetry (CV) was performed using a CHI604A electrochemical work station (CH Instrument, Shanghai) at a scan rate of 0.5 mV s⁻¹ within the potential range of 0–2 V (vs. Li/Li⁺).

3. RESULTS AND DISCUSSION

X-ray diffraction patterns of the as-deposited Sn-Cu alloys and nanoporous Sn-Cu alloys are shown in Fig. 1.

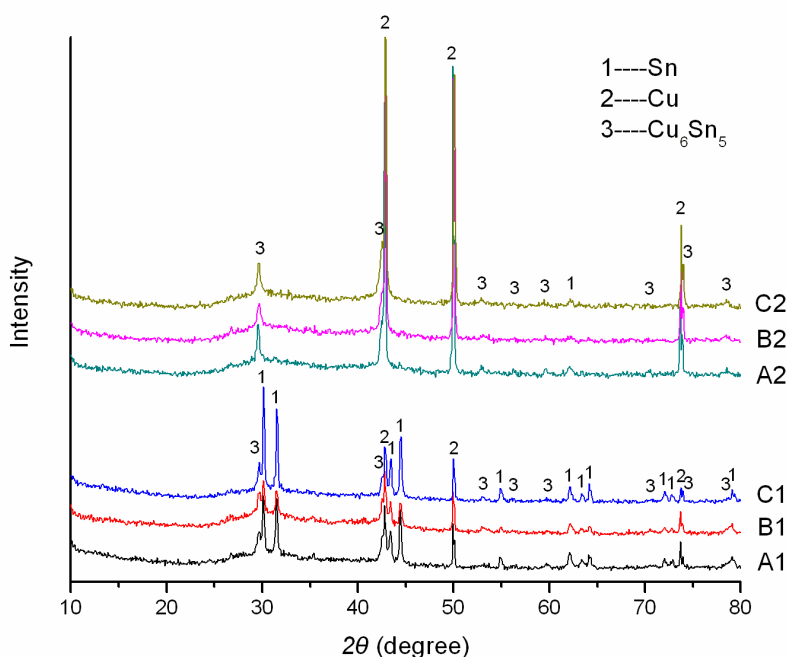


Figure 1. XRD patterns of the as-deposited Sn-Cu alloys and nanoporous Sn-Cu alloys

For the three as-deposited Sn-Cu alloys, the characteristic diffraction peaks of Sn (PDF card No.04-0673) can be clearly seen at 30.6°, 32.0°, 43.9°, 44.9°, 55.3°, 62.5°, 63.8°, 64.6°, 72.4°, 73.2° and 79.5°. But these peaks can not be observed in the patterns of the nanoporous Sn-Cu alloys. This demonstrates that a lot of Sn phase has lost during electrochemical dealloying process. Cu₆Sn₅ phase as evidenced by the diffraction peaks at 2θ of 30.1° and 43.0° with monoclinic structure presents in every sample. In addition, the diffraction peaks of copper located at 43.3°, 50.4° and 74.1° can be also observed. The diffraction intensity of copper peaks became more evident after electrochemical dealloying, reflecting decrease in thickness of the alloy layer after electrochemical dealloying. These results indicated that the alloy with active Sn and Cu₆Sn₅ phases formed during electroplating, and a lot of Sn phase in the alloys dissolved during electrochemical dealloying process with Cu₆Sn₅ phase left.

Table 2. The composition of the Sn-Cu alloys before and after electrochemical dealloying

Alloys	Mass (mg)		Molar Ratio (%)	
	Sn	Cu	Sn	Cu
A1	27.9	3.21	82.3	17.7
A2	8.03	3.27	56.8	43.2
B1	26.1	3.54	79.8	20.2
B2	9.46	3.44	59.5	40.5
C1	25.2	3.70	78.5	21.5
C2	13.6	3.34	68.5	31.5

AAS was used to determine the composition of the alloys before and after electrochemical dealloying and the results are listed in Table 2.

As expected, the Sn content in the as-deposited alloys decreased with the decreasing concentration of SnSO_4 in the plating bath. After dealloying, the Sn content in the residual nanoporous Cu-Sn alloy decreased significantly, while the copper content remain nearly unchanged. This result is in good accordance to the fact shown in Fig. 1 that the diffraction peaks corresponding to Sn phase disappear after dealloying. The diffraction peaks relating to Cu_6Sn_5 still exist after electrochemical dealloying, suggesting easier dissolution of Sn phase than Cu_6Sn_5 phase. So the increased content of tin in A2, B2 and C2 can be attributed to the increased content of Cu_6Sn_5 phase in A1, B1 and C1.

The color of the as-deposited Cu-Sn alloys was grey. After electrochemical dealloying, the color of them turned black. The color change reflects the morphology change of the residual Cu-Sn alloy. The SEM images of the as-deposited Cu-Sn alloys before and after electrochemical dealloying are shown in Fig. 2.

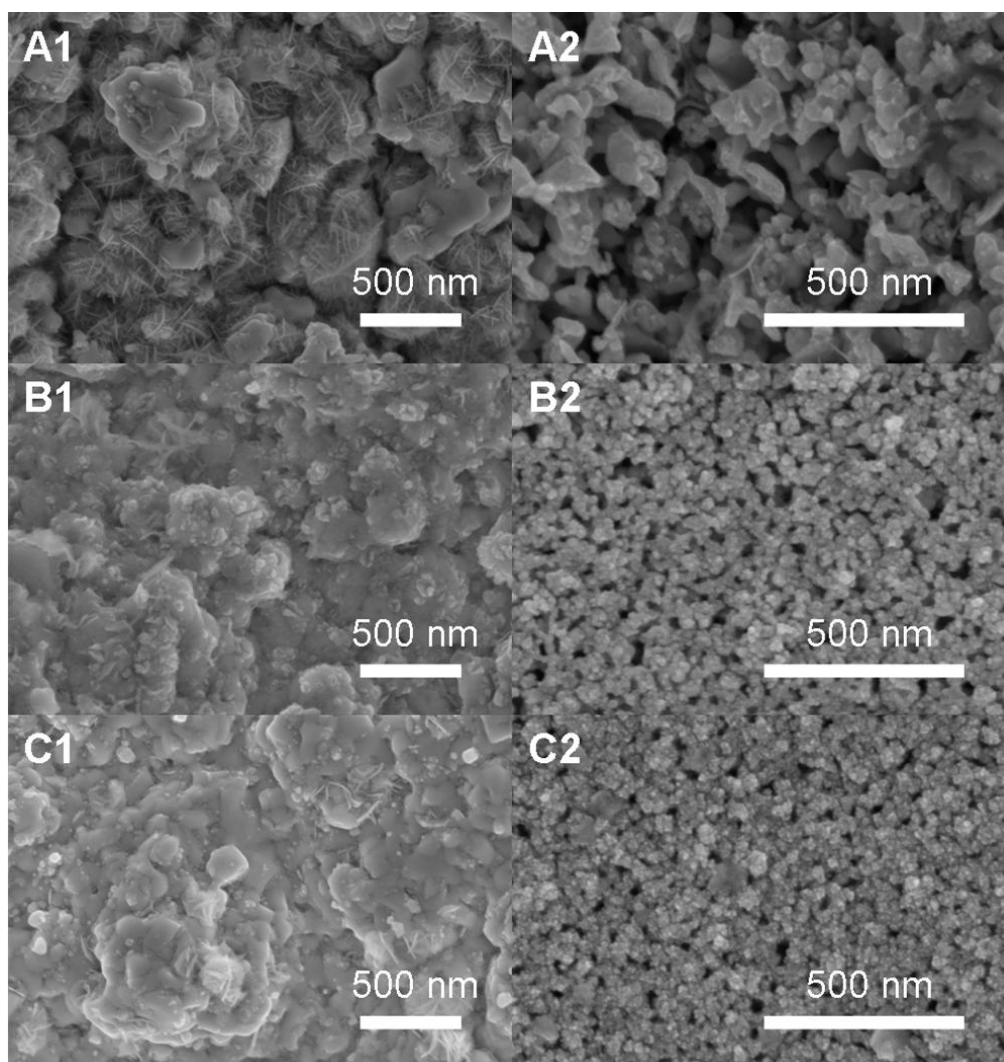


Figure. 2 SEM images of the Sn-Cu alloys before and after electrochemical dealloying

Fig.2 shows that the structure of the as-deposited Sn-Cu alloy is firm with rough surface. After electrochemical dealloying, the residual Sn-Cu alloy become porous and its surface become smoother, showing electrochemical leveling effect. Formation of nanopore accounts for the color change from grey to black before and after electrochemical dealloying. For A1, some Sn dendrites present and only a few large pores formed in A2 matrix. The large porous structure of A2 is not as good as we expected. According to AAS results shown in Table 2, the loss of Sn content from A1 during electrochemical dealloying is the highest. The fact that the highest Sn loss only leaves large pore suggests presence of large Sn phase in A1 alloy. The large Sn phase can be ascribed to the high concentration of SnSO₄ in the electroplating bath. On the other hand, the dentrite morphology is not suitable for constructing bi-continuous porous structure. Therefore, we reduced SnSO₄ concentration in the electroplating bath so as to reduce the size of deposited Sn particle. As can be seen form Fig. 2, the pore size formed in B2 and C2 reduced remarkably. The pores formed in B2 and C2 are of irregular shape with the pore size around 50 nm. The porosity of C2 is relative lower, which can be ascribed to the low Sn content in C1 alloy. Hence, it is not enough for C2 to hold enough electrolyte solution and provide large active surface for electrochemical reaction. According to our expectation, the porosity and pore structure of B2 are much suitable for use as negative materials for LIB. This expectation is testified by both cyclic voltammetry and charge-discharge cycling test. The CV measurements were conducted with the first five cycles shown in Fig. 3.

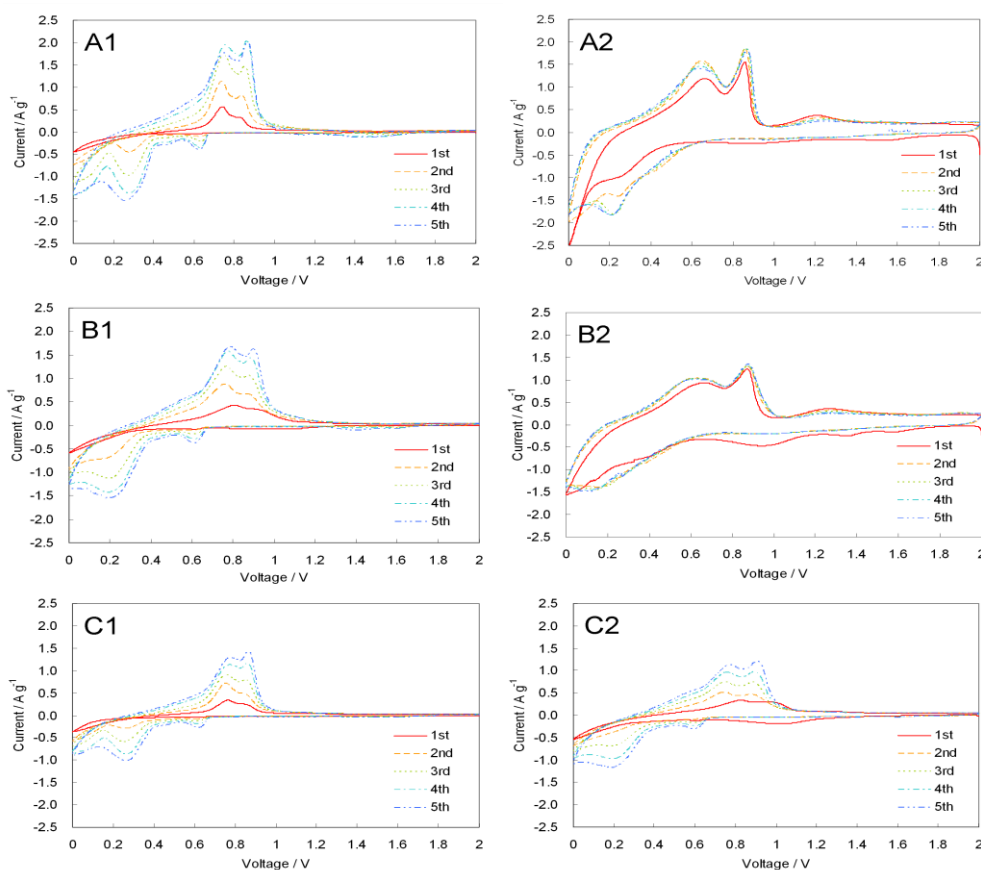


Figure 3. Cyclic voltammograms of A1, A2, B1, B2, C1, and C2

For A1, B1, C1 and C2, there are two reduction peaks appearing at ca. 0.6 V and 0.3 V in the negative-going scan and two oxidation peaks occurring at ca. 0.9 V and 0.7 V in the positive-going scan. The two pairs of redox peaks correspond to the lithiation of Sn to form Li_xSn ($x < 2.33$) and further lithiation to form Li_ySn ($3.5 < y < 4.4$) [21]. In the first cycle, both reduction and oxidation peaks can not be observed for the serious polarization of the new electrode. But for A2 and B2, the main reactions are different. The two reduction peaks close to 0.2 V and 0 V stand for lithiation of Cu_6Sn_5 to Li_2CuSn and further formation of $\text{Li}_{4.4}\text{Sn}$, and the oxidation peaks at ca. 0.8 V and 0.6 V relevant to the reverse process [22].

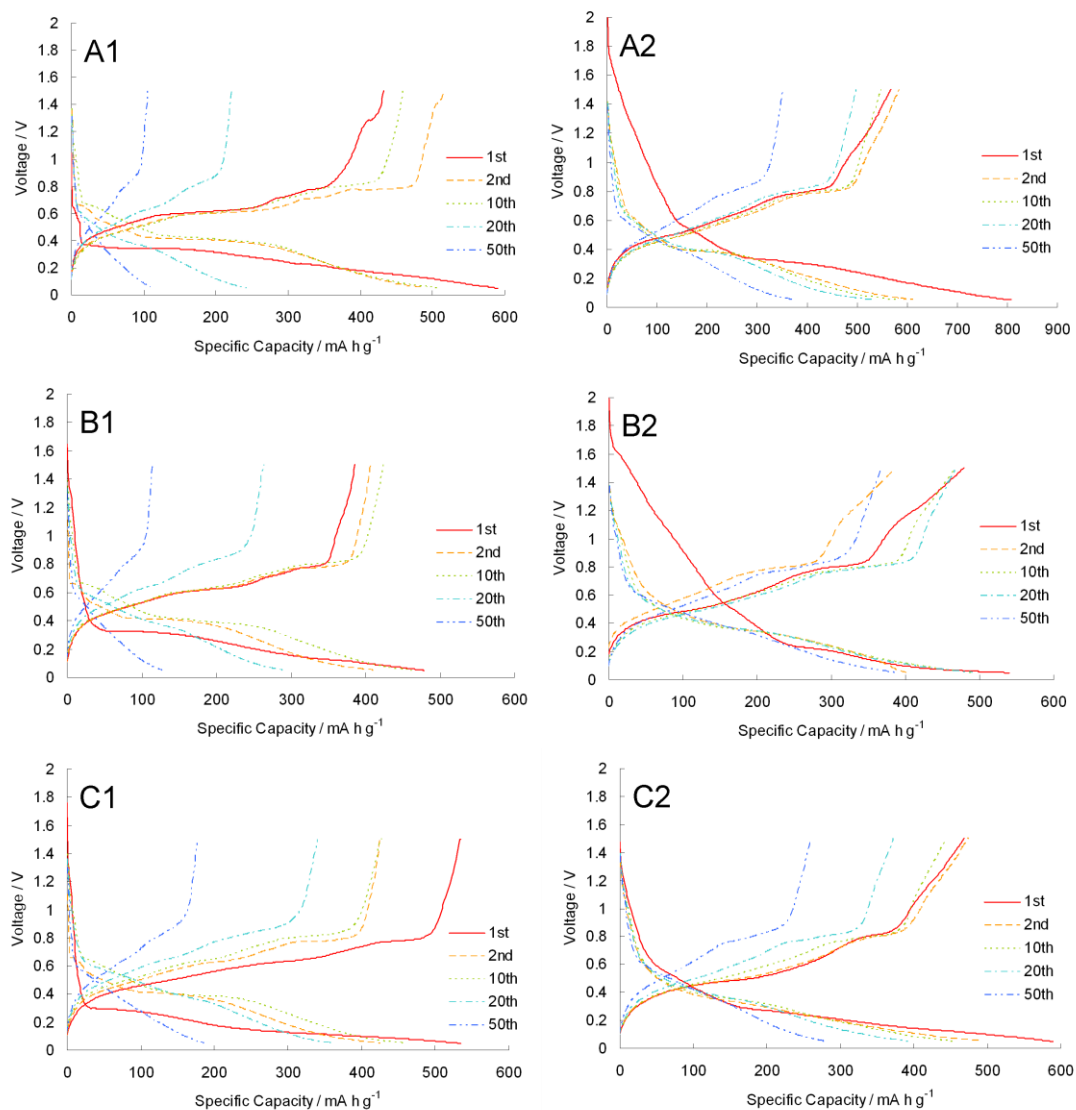


Figure 4. Charge and discharge curves of A1, A2, B1, B2, C1 and C2 alloys

The reversibility of A2 and B2 is much better than the others as shown by the coincidence of CV curves during the first five cycles. The better reversibility reflects the improved structure stability of A2 and B2 due to formation of nanoporous. That the peak current increases with cycling can be due to continuous formation of new surface so that more and more active material were involved in

lithiation. This phenomenon is obvious in the A1, B1 and C1. It also happened in C2 for the specific surface area is not big enough. Owing to the larger specific surface area, the oxide covering nanoporous Sn-Cu alloys is much more than that covering the as-deposited alloys. The reduction peak appearing between 0.6 V and 1.2 V in the first circle corresponds to the reduction of surface oxide. Another significant difference in CV between as-deposited alloys and nanoporous alloys appears appear in 1.5-2.0 V range. The large separation between the forward and reverse scan of A2, B2 and C2 reflects a large capacitance. This is another evidence for large specific surface area formed after electrochemical dealloying.

The charge-discharge curves of Sn-Cu alloys before and after electrochemical dealloying were shown in Fig.4.

In Fig. 4, three pairs of platforms appear in the charge and discharge curves for A1, B1 and C1. The platforms appearing at 0.65 V, 0.51 V and 0.41 V in the discharge curve corresponds to the platforms appearing at 0.77 V, 0.71 V and 0.63 V in the charge curve. These three pairs of platforms relate to the formation and disappearance of $\text{Li}_{0.4}\text{Sn}$, LiSn , and $\text{Li}_{2.33}\text{Sn}$ phases, respectively [2, 21]. Because a lot of Sn phase has lost during electrochemical dealloying, the nanoporous Sn-Cu alloys show different platforms in the charge and discharge curve. The platforms appearing at about 0.4 V and 0.1 V in the discharge curve corresponds to that appearing at 0.8 V and 0.5 V in the charge curve. The former platform relates to alloying of Cu_6Sn_5 to form Li_2CuSn and the later for further alloying of Li_2CuSn to $\text{Li}_{4.4}\text{Sn}$ [22]. Polarization of as-deposited Sn-Cu alloys in the first discharge is more obvious than that of nanoporous Sn-Cu alloy, reflecting increased surface area after electrochemical dealloying. The irreversible capacity of nanoporous Sn-Cu alloy samples above 0.8 V in the first discharge curve is much more than that of as-deposited samples. This irreversibility can be ascribed to reduction of more oxide and formation of solid-electrolyte interphase (SEI) membrane over large surface[23].

The cycling performance of the Sn-Cu alloys is shown in Fig. 5.

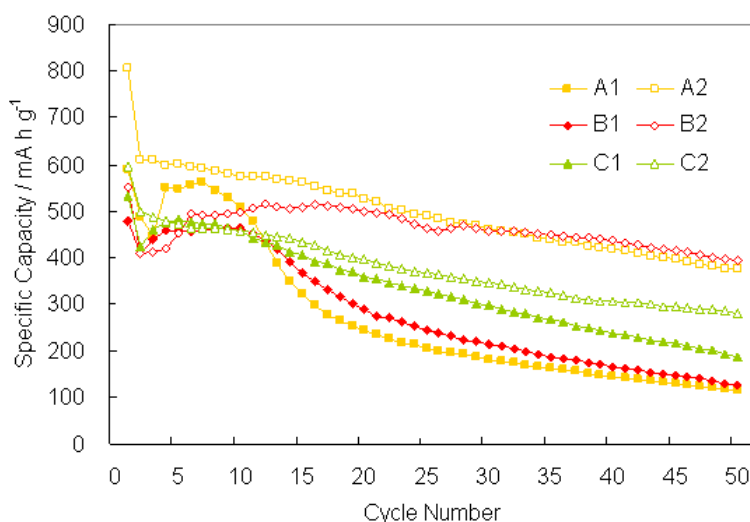


Figure 5. Transition of specific capacity with cycle number for different Sn-Cu alloys

According to Fig. 5, the initial specific capacity of the six Cu-Sn alloys are 591 mA h g⁻¹ (A1), 807 mA h g⁻¹ (A2), 479 mA h g⁻¹ (B1), 550 mA h g⁻¹ (B2), 534 mA h g⁻¹ (C1) and 596 mA h g⁻¹ (C2). After 50 cycles, the specific capacity of A1, B1 and C1 are 114 mA h g⁻¹, 126 mA h g⁻¹ and 185 mA h g⁻¹. For the nanoporous Sn-Cu alloys, their specific capacities keep in 375 mA h g⁻¹, 388 mA h g⁻¹, and 278 mA h g⁻¹, respectively after 50 cycles. Nanoporous Sn-Cu alloy show an improved cycling performance than as-deposited Sn-Cu alloys. Although nanoporous Sn-Cu alloys have low Sn content than as-deposited samples, they have similar initial capacity but improved cycling performance. The decay of capacity with cycling slows down with increasing copper content and porosity of the alloy. We attributed the improved capacity retention to the porous structure of these alloy. The porous structure enlarges the contact area of alloy with electrolyte, makes more material involved in lithiation reaction, and provides more room to tolerate volume fluctuation during cycling. The improved capacity retention also relates to the enrichment of Cu₆Sn₅ phase in the nanoporous Sn-Cu alloy. Although Cu₆Sn₅ also presents in the as-deposited alloys, with the serious expansion of Sn phase, the structural stability of the as-deposited alloy deteriorate rapidly. After removal most Sn phase by electrochemical dealloying, the Cu₆Sn₅ phase with better volume stability becomes the main component of the active materials, which benefits the cycling performance. Therefore, we attribute the cycling improvement to mutual effect of many factors such as introduction of inert alloy component, removal of Sn phase with large volume expansion, formation of room in the alloy matrix to buffer volume expansion, and enlargement of surface area. The best cycling retention of B2 as we expect support this postulation.

4. CONCLUSIONS

Nanoporous Sn-Cu alloy materials with different Sn content, different porosity and different pore size were prepared by electroplating-electrochemical dealloying method on the Cu foil substrate. The nanoporous Sn-Cu alloys show an improved specific capacity and better cycling performance. The improvement is mutual effect of many factors. The combination of inert alloy component and porous structuring is an effective way to improve capacity and cycling performance of Sn-Cu alloys.

ACKNOWLEDGEMENTS

This work was financially supported by Natural Science Foundation of Shandong Province (Project No. ZR2009BM012) and National Basic Research Program of China (No.2011CB935901)

References

1. M. Armand and J.M. Tarascon, *Nature*, 451 (2008) 652.
2. M. Winter and J.O. Besenhard, *Electrochimica Acta*, 45 (1999) 31.
3. A. Sivashanmugam, T.P. Kumar, N.G. Renganathan, S. Gopukumar, M. Wohlfahrt-Mehrens and J. Garche, *J. Power Sources*, 144 (2005) 197.
4. K. Ui, S. Kikuchi, Y. Kadoma, N. Kumagai and S. Ito, *J. Power Sources*, 189 (2009) 224.

5. L. Huang, H.B. Wei, F.S. Ke, X.Y. Fan, J.T. Li, S.G. Sun, *Electrochim. Acta*, 54 (2009) 2693.
6. F. Ke, L. Huang, H. Jiang, H. Wei, F. Yang and S. Sun, *Electrochem. Commun.*, 9 (2007) 228.
7. N. Tamura, R. Ohshita, M. Fujimoto, S. Fujitani and M. Kamino, *J. Power Sources*, 107 (2002) 48.
8. J.C. Lytle, H. Yan, N.S. Ergang, W.H. Smyrl and A. Stein, *J. Mater. Chem.*, 14 (2004) 1616.
9. Z. Chen, J. Qian, X. Ai, Y. Cao and H. Yang, *J. Power Sources*, 189 (2009) 730.
10. X.Y. Fan, F.S. Ke, G.Z. Wei, L. Huang and S.G. Sun, *J. Alloys Compd.*, 476 (2009) 70.
11. G. Derrien, J. Hassoun, S. Panero and B. Scrosati, *Adv. Mater.*, 19 (2007) 2336.
12. C. Kim, M. Noh, M. Choi, J. Cho and B. Park, *Chem. Mater.*, 17 (2005) 3297.
13. X.Y. Fan, F.S. Ke, G.Z. Wei, L. Huang and S.G. Sun, *Electrochem. Solid-State Lett.*, 11 (2008) A195.
14. R. Kim, D. Nam and H. Kwon, *J. Power Sources*, 195 (2010) 5067.
15. Q. Li, S. Hu, H. Wang, F. Wang, X. Zhong and X. Wang, *Electrochim. Acta*, 54 (2009) 5884.
16. Z. Du, S. Zhang, T. Jiang and Z. Bai, *Electrochim. Acta*, 55 (2010) 3537.
17. L. Xue, Z. Fu, Y. Yao, T. Huang and A. Yu, *Electrochim. Acta*, 55 (2010) 7310.
18. H. Zhao, C. Jiang, X. He, J. Ren and C. Wan, *Ionics*, 14 (2008) 113.
19. Y. Yu, L. Gu, C. Zhu, P.A.v. Aken and J. Maier, *J. AM. CHEM. SOC.*, 131 (2009) 15984.
20. Y. Yu, L. Gu, X. Lang, C. Zhu, T. Fujita, M. Chen and J. Maier, *Adv. Mater.*, 23 (2011) 2443.
21. R.A. Huggins, *J. Power Sources*, 81-82 (1999) 13.
22. S. Liu, Q. Li, Y. Chen and F. Zhang, *J. Alloys Compd.*, 478 (2009) 694.
23. N. Pereira, L.C. Klein and G.G. Amatucci, *Solid State Ionics*, 167 (2004) 29